

# Simulation of Rodlike Particles in Field-Flow Fractionation (FFF)<sup>a</sup>

Frederick R. Phelan Jr. and Barry J. Bauer  
Polymers Division, NIST,  
Gaithersburg, MD 20899

## Introduction

The manufacturing of single wall carbon nanotubes (SWNTs) results in mixtures that are polydisperse with respect to both size and chirality<sup>b</sup>, the latter of which strongly affects the tube electronic properties<sup>c</sup>. For nanotubes to achieve their full potential in applications, it is desirable to be able to separate them according to both of these physical characteristics. Field-flow fractionation (FFF) (1-3) is an liquid based technique used to separate various macromolecular, colloidal, and particulate materials ranging from  $10^{-3}$  to  $10^2$   $\mu\text{m}$  in size and has recently been applied in a number of studies (4-9) to the separation of nanotubes. In FFF, a mixture to be separated is driven through a channel (the “flow”, in FFF) while a field is applied in a direction perpendicular to the streamwise direction. The perpendicular field may be either another flow field, an electric field, or a temperature gradient, amongst a number of possibilities. The perpendicular field is chosen so that the interaction between the field and the streamwise parabolic profile, promotes a separation of components based on their mobility in the field.

In this work, we develop a Brownian dynamics simulation of prolate ellipsoidal particles to investigate the separation of rodlike particles in FFF. The particle motions are governed by stochastic forms of a linear momentum balance with orientation dependent drag and diffusion coefficients, and the Jeffery equation with rotational diffusion (10; 11). The simulation shows that nanotube scale particles would be expected to elute by a normal mode mechanism, based on a particle diameter of 1 nm. Elution profiles and average velocity through the device as a function of particle size, and throughput and cross flow flowrates are examined.

## FFF Theory and Practice

### *Normal Mode Separations in flow-FFF*

Classical flow-FFF, shown in Figure 1, is a separation technique in which a perpendicular cross flow is imposed upon a parabolic channel flow of a dilute solution of macromolecular, colloidal or particulate material. The cross flow exits through a porous accumulation wall which is impermeable to the particulates. Separation is achieved due to the different residence times of the particles based upon their position in the parabolic velocity profile in the throughput direction. In practice, the length,  $L$ , of

---

<sup>a</sup> Official contribution of the National Institute of Standards and Technology; not subject to copyright in the United States.

<sup>b</sup> A carbon nanotube is like a cylinder rolled up from a single sheet of graphite, whose atoms are arranged in hexagons. Rolling the lattice at different angles creates a visible twist or spiral in the nanotube's molecular structure. This twist is called chirality.

<sup>c</sup> e.g., <http://www.ncnr.nist.gov/staff/taner/nanotube/types.html>. For a given  $(n,m)$  nanotube, if  $2n + m = 3q$  (where  $q$  is an integer), then the nanotube is metallic, otherwise the nanotube is a semiconductor.

the flow channel is much greater than the gap width,  $H$ . Gap widths on the order of 10 to 100  $\mu\text{m}$  are typically used (1).

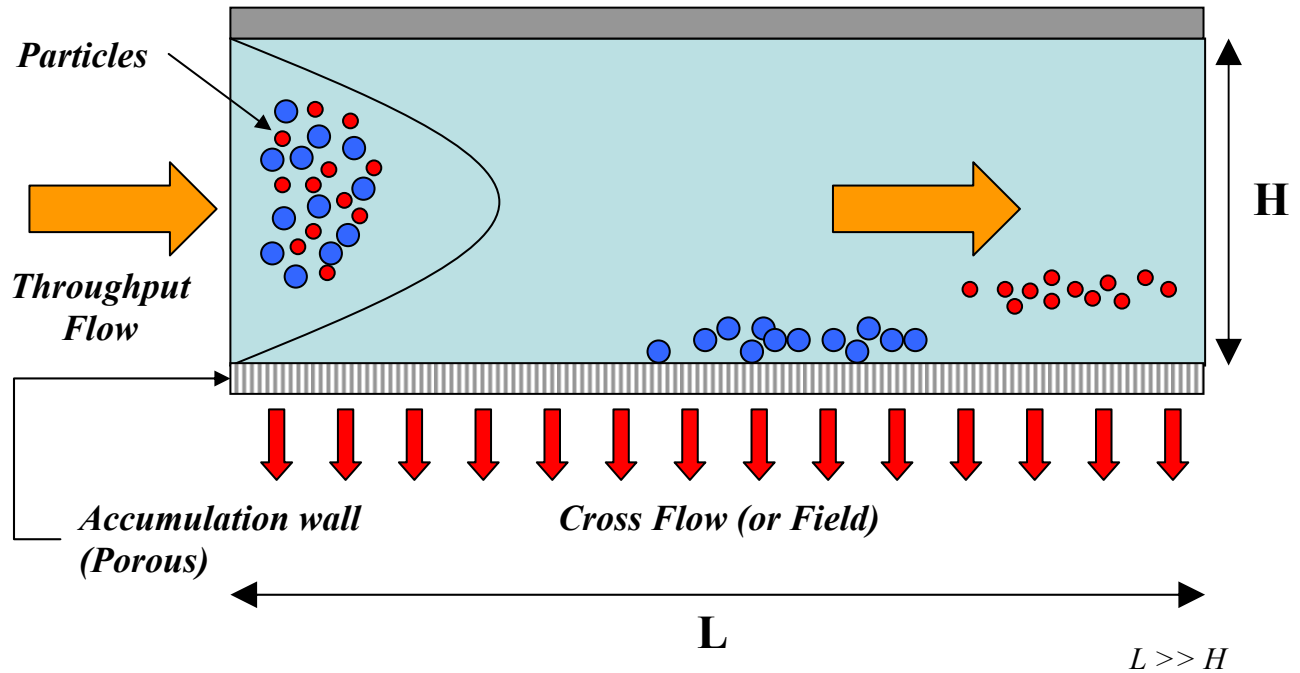


Figure 1 – Classical field-flow fractionation. The velocity profile in the throughput direction is parabolic, and the cross flow velocity is uniform.

A number of different mechanisms can be exploited to achieve separation in FFF (1-3). What is termed normal mode separation applies to particles which are small enough to undergo significant Brownian motion. Because the solutions are dilute, the main forces acting on the particles are the drag force and the Brownian force, as shown in Figure 2.

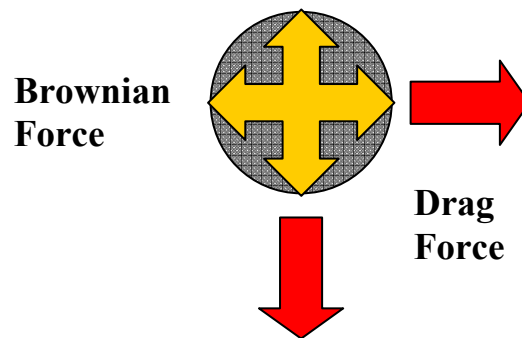


Figure 2 – Forces acting on particles in dilute solutions in FFF.

Under these conditions, smaller particles which are more diffusive and experience less drag, travel with an average position closer to the centerline as pictured in Figure 3.

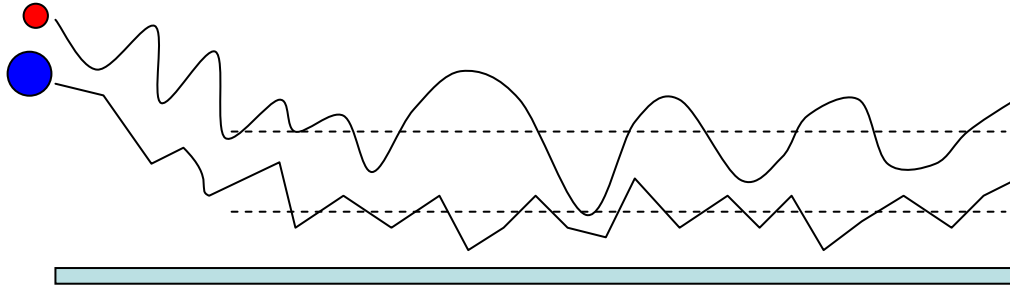


Figure 3 – In normal mode FFF, smaller particles which are more diffusive and experience less drag, have an average position closer to the centerline.

For an ensemble of particles, this competition between advection and diffusion in the cross flow direction drives particles of different sizes to discrete equilibrium layers. Smaller particles have average positions closer to the centerline, and thus elute faster than larger particles, as pictured in Figure 4.

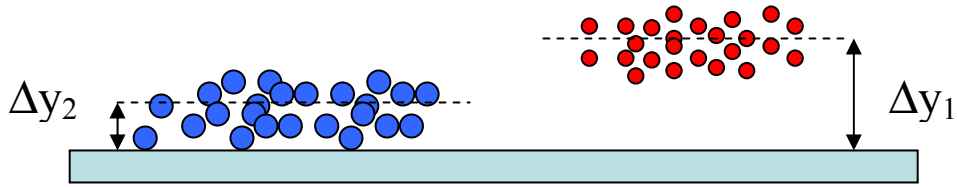


Figure 4 – Equilibrium bands for normal mode separation in FFF. Bands with an average position closer to the center elute more quickly.

### ***Normal Mode Retention***

The competition between advection and diffusion in the cross flow direction leads particles to an equilibrium concentration profile in the gap direction given by (1-3)

$$\frac{c}{c_0} = \exp\left(-\frac{y}{\ell}\right) \quad (1.1)$$

where  $c_0$  is the concentration of the particles at the accumulation wall,  $\ell$  is a characteristic length given by

$$\ell = \frac{|v_c|}{D} \quad (1.2)$$

$v_c$  is the average cross flow velocity, and  $D$  is the diffusion coefficient of the particle in the cross flow direction.

The total retention time,  $t_r$ , of the particles can be computed by integrating the concentration profile over the length of the channel. Assuming a parabolic velocity profile,  $u(y)$ , for flow in the throughput direction, the retention time is given by

$$\frac{t_r}{t_0} = \frac{1}{R} \quad (1.3)$$

where  $t_0$  is the average residence time of non-retained tracers

$$t_0 = \frac{L}{\bar{u}} \quad (1.4)$$

$R$  is called the Retention and is given by

$$R = 6\lambda \left[ \coth\left(\frac{1}{2\lambda}\right) - 2\lambda \right] \quad (1.5)$$

where  $\lambda$  is an inverse Peclet Number ( $Pe$ ) given by

$$\lambda = \frac{D}{|v_c|H} = \frac{1}{Pe} \quad (1.6)$$

The Retention is a dimensionless variable whose value is bounded in the range  $0 < R < 1$ . In the limit,  $R = 0$  particles are trapped on the accumulation wall, and thus, this corresponds to the case of zero elution. As  $R$  increases, the average speed at which particles elute also increases approaching the minimum  $t_0$  at  $R = 1$ . Thus, the ability to separate particles depends on the relative Retention values of the different particles dispersed in the solution.

For spherical particles, the Einstein diffusion coefficient is given by  $D = \frac{kT}{\zeta}$  where  $\zeta = 6\pi r\eta$  is the Stokes' law drag coefficient,  $r$  is the radius of the particle,  $\eta$  is the viscosity of the fluid,  $k$  is Boltzmann's constant, and  $T$  is the absolute Temperature. A plot of the Retention for spheres of various sizes is shown in Figure 5 using some typical operating conditions for FFF given in Table 1.

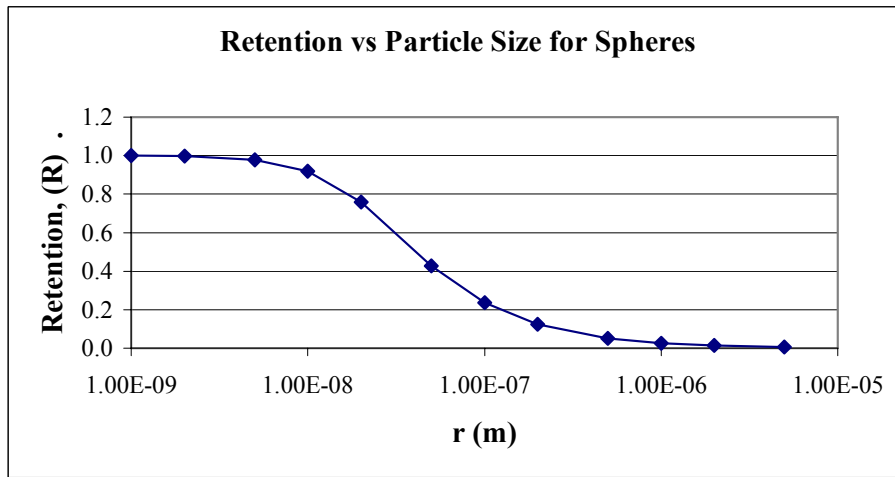


Figure 5 – A plot of the Retention variable for spherical particles under typical conditions in FFF.

L (m)	W (m)	H (mm)	Cross Flow Rate (m <sup>3</sup> /s)	Viscosity (Pa-s)	Temperature (K)
0.2	0.1	1	1 x 10 <sup>-9</sup>	0.001	293

Table 1 – Typical operating conditions for separations in FFF.

## Brownian Dynamics Simulation

### General Theory

The motion of a particle immersed in a flowing liquid is governed by two equations, conservation of linear momentum (Newton's second law) and conservation of angular momentum. In the context of the present work, the two most basic forces that act on the particle are drag forces which arise due to the action of the stress in the fluid on the particle, and the random Brownian force, which arises due to the molecular motion of the fluid on the particle. In terms of these forces, the respective conservation equations may be written without loss of generality as

$$m \frac{d\mathbf{U}}{dt} = -\mathbf{F}_D(t) + \mathbf{F}_B(t) + \sum_j \mathbf{F}_{\{j\}} \quad (2.1)$$

$$\underline{\underline{M}} \cdot \frac{d\mathbf{\Omega}}{dt} = -\mathbf{T}_D(t) + \mathbf{T}_B(t) + \sum_j \mathbf{T}_{\{j\}} \quad (2.2)$$

where  $m$  is the mass of the particle,  $\underline{\underline{M}}$  is the moment of inertia tensor,  $\mathbf{U}$  is the velocity of the particle,  $\mathbf{\Omega}$  is the angular momentum of the particle,  $\mathbf{F}_D(t)$  is the fluid-particle drag force,  $\mathbf{F}_B(t)$  is a random force due to Brownian motion,  $\mathbf{T}_D(t)$  is a drag induced torque,  $\mathbf{T}_B(t)$  is a random torque due to Brownian motion, and  $\sum_j \mathbf{F}_{\{j\}}$  and  $\sum_j \mathbf{T}_{\{j\}}$  represent other forces and torques acting on the particle.

The drag force and torque exerted by the particle on the ambient fluid may be evaluated in terms of the fluid stress, and are given by

$$\mathbf{F}_D = - \int_{S_p} (\hat{\mathbf{n}} \cdot \underline{\underline{\tau}}) dS \quad (2.3)$$

$$\mathbf{T}_D = - \int_{S_p} (\underline{\underline{r}} - \underline{\underline{r}}_c) \times (\hat{\mathbf{n}} \cdot \underline{\underline{\tau}}) dS \quad (2.4)$$

where  $\underline{\underline{\tau}}$  is the stress tensor of the fluid,  $\hat{\mathbf{n}}$  is the unit normal vector directed outwardly from the surface,  $S_p$  denotes the surface of the particle, and  $\underline{\underline{r}}_c$  is the position vector of the particle at its center of mass.

When the concentration of particles in a fluid is dilute, the forces and torques given by Eqs. (2.3)-(2.4) do not significantly alter the flow field, and the motion of the particles governed by Eqs. (2.1)-(2.2) may be calculated independently of the Navier-Stokes equations which govern the motion of the fluid. However, when the particles are of sufficient concentration, the forces and torques generated by the particle alter the flow field. This couples Eqs. (2.1)-(2.2) with the solution for the motion of the fluid. In this case, the stresses generated in the fluid must be incorporated into the momentum balance for the fluid in order to obtain a solution to the problem. This is done by calculating the stresslet, which is the stress generated by the particles in the fluid. The stresslet is given by the equation

$$\underline{\underline{S}} = - \frac{1}{2} \int_{S_p} \left\{ (\underline{\underline{r}} - \underline{\underline{r}}_c) (\hat{\mathbf{n}} \cdot \underline{\underline{\tau}}) + (\hat{\mathbf{n}} \cdot \underline{\underline{\tau}}) (\underline{\underline{r}} - \underline{\underline{r}}_c) - \frac{2}{3} (\hat{\mathbf{n}} \cdot \underline{\underline{\tau}}) \cdot (\underline{\underline{r}} - \underline{\underline{r}}_c) \mathbf{I} \right\} dS \quad (2.5)$$

Analytical relationships for drag force, torque and the stresslet for a number of particle types are given in a number of references (10; 11).

## Modeling of Rodlike Particles

Separations in flow-FFF are usually conducted with very dilute, aqueous solutions. Thus, in developing a process model we make the assumptions of Newtonian solvent rheology and negligible excluded volume effects (12; 13). In addition, because the aspect ratio of the particles is large, hydrodynamic interactions may be neglected as well (14). To model the drag force generated by the particles in the flow, the nanotubes are modeled as prolate ellipsoids (10; 11), shown in Figure 6. A prolate ellipsoid is formed by the rotation of an ellipse about its major axis. The object has a major axis of length,  $2a$ , a minor axis of length,  $2b$ , and is symmetric to the minor axis in the third direction. The orientation vector  $\underline{p}$  describes the direction of the major axis in 3-D space.

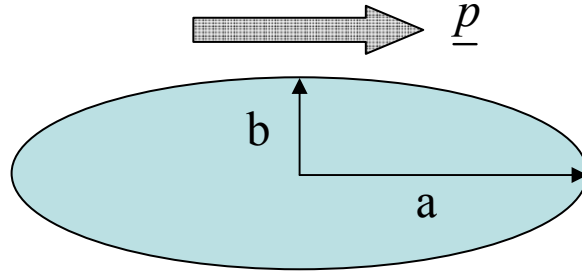


Figure 6 – Model parameters and orientation vector for the prolate ellipsoid.

Because the particles rotate in the flow, and the drag force is orientation dependant and described by the relation (10; 11)

$$\underline{F}_D^{(i)}(t) = \underline{\underline{\zeta}}^{(i)} \cdot (\underline{U}^{(i)} - \underline{v}) \quad (2.6)$$

where for prolate ellipsoids the resistance matrix  $\underline{\underline{\zeta}}^{(i)}$  is described in terms of the orientation vector by the relations

$$\underline{\underline{\zeta}}^{(i)} = \eta \left\{ \left( X_A^{(i)} - Y_A^{(i)} \right) \underline{p}^{(i)} \underline{p}^{(i)} + Y_A^{(i)} \underline{\underline{I}} \right\} \quad (2.7)$$

$$\frac{X_A}{6\pi a} = \frac{8}{3} \cdot \frac{s^3}{-2s + (1+s^2)L} \quad (2.8)$$

$$\frac{Y_A}{6\pi a} = \frac{16}{3} \cdot \frac{s^3}{2s + (3s^2 - 1)L} \quad (2.9)$$

$$L = \ln \frac{(1+s)}{(1-s)} \quad (2.10)$$

In a similar manner, the drag-torque in the angular momentum balance is given by

$$\underline{\underline{T}}_D^{(i)}(t) = \underline{\underline{\zeta}}^{(i)} \cdot (\underline{\underline{\Omega}}^{(i)} - \underline{\underline{\omega}}) + \underline{\underline{\chi}}^{(i)} : \underline{\underline{D}} \quad (2.11)$$

in which  $\underline{\underline{D}}$  and  $\underline{\underline{\omega}}$  are the fluid stretching tensor and angular velocity vector (i.e., one half the vorticity), respectively, given by

$$\underline{\underline{D}} = \frac{1}{2} (\nabla \underline{v} + \nabla \underline{v}^T) \quad (2.12)$$

$$\underline{\omega} = \frac{1}{2} \nabla \times \underline{v} \quad (2.13)$$

and the resistance matrices  $\underline{\underline{\zeta}}^{(i)}$  and  $\underline{\underline{\chi}}^{(i)}$  are defined by the relations

$$\underline{\underline{\zeta}}^{(i)} = \eta \left\{ (X_C^{(i)} - Y_C^{(i)}) \underline{p}^{(i)} \underline{p}^{(i)} + Y_C^{(i)} \underline{I} \right\} \quad (2.14)$$

$$\underline{\underline{\chi}}^{(i)} = \eta Y_H^{(i)} (\underline{\underline{\varepsilon}} \cdot \underline{p}^{(i)} \underline{p}^{(i)}) \quad (2.15)$$

$$\frac{X_C}{6\pi a^3} = \frac{4}{3} \cdot \frac{s^3 (1-s^2)}{2s - (1-s^2)L} \quad (2.16)$$

$$\frac{Y_C}{6\pi a^3} = \frac{4}{3} \cdot \frac{s^3 (2-s^2)}{-2s + (1+s^2)L} \quad (2.17)$$

$$\frac{Y_H}{6\pi a^3} = \frac{4}{3} \cdot \frac{s^5}{-2s + (1+s^2)L} \quad (2.18)$$

where  $\underline{\underline{\varepsilon}}$  is third-order Levi-Civita tensor.

Under the assumptions of negligible translational and rotational inertia, i.e.,  $m \frac{d\underline{U}}{dt} \approx 0$  and  $M \frac{d\underline{\Omega}}{dt} \approx 0$ , the governing equations for an ensemble of prolate ellipsoids, individually denoted by the superscript  $(i)$ , can be written as

$$\frac{d\underline{R}^{(i)}}{dt} = \underline{v}(\underline{R}^{(i)}) + \left[ \underline{\underline{\zeta}}^{(i)} \right]^{-1} \cdot \left( \underline{F}_B^{(i)}(t) + \sum_j \underline{F}_j^{(i)} \right) \quad (2.19)$$

$$\frac{d}{dt} (\underline{p}^{(i)}) = -\underline{W} \cdot \underline{p}^{(i)} + \lambda_p (\underline{D} \cdot \underline{p}^{(i)} - \underline{D} : \underline{p}^{(i)} \underline{p}^{(i)}) + \underline{p}^{(i)} \times \left[ \underline{\underline{\zeta}}^{(i)} \right]^{-1} \cdot \left( \underline{T}_B^{(i)}(t) + \sum_j \underline{T}_j^{(i)} \right) \quad (2.20)$$

where  $\underline{W}$  is the vorticity tensor given by

$$\underline{W} = \frac{1}{2} (\nabla \underline{v} - \nabla \underline{v}^T) \quad (2.21)$$

and the quantity  $\lambda_p$  is a function of the particle aspect ratio,  $\mathfrak{R} = \frac{a}{b}$ , according to

$$\lambda_p = \frac{\mathfrak{R}^2 - 1}{\mathfrak{R}^2 + 1} \quad (2.22)$$

The resistance matrices have the analytical inverses

$$\left[ \underline{\underline{\zeta}}^{(i)} \right]^{-1} = \frac{1}{\eta} \left\{ \left( \frac{1}{X_A^{(i)}} - \frac{1}{Y_A^{(i)}} \right) \underline{p}^{(i)} \underline{p}^{(i)} + \frac{1}{Y_A^{(i)}} \underline{I} \right\} \quad (2.23)$$

$$\left[ \underline{\underline{\zeta}}^{(i)} \right]^{-1} = \frac{1}{\eta} \left\{ \left( \frac{1}{X_C^{(i)}} - \frac{1}{Y_C^{(i)}} \right) \underline{p}^{(i)} \underline{p}^{(i)} + \frac{1}{Y_C^{(i)}} \underline{I} \right\} \quad (2.24)$$

These equations for the particle motions can be described as a stochastic form of the linear momentum balance with orientation dependent drag and diffusion coefficients, and a stochastic form of the Jeffery equation with rotational diffusion (10; 11). In order for the dynamics to satisfy the

fluctuation-dissipation theorem, the values for the Brownian forces and torques must satisfy the relationships

$$\langle \underline{F}_B^{(i)}(t) \rangle = 0 \quad (2.25)$$

$$\langle \underline{T}_B^{(i)}(t) \rangle = 0 \quad (2.26)$$

$$\langle \underline{F}_B^{(i)}(t) \underline{F}_B^{(i)}(t') \rangle = 2kT \underline{\underline{\zeta}}^{(i)} \delta(t-t') \quad (2.27)$$

$$\langle \underline{T}_B^{(i)}(t) \underline{T}_B^{(i)}(t') \rangle = 2kT \underline{\underline{\xi}}^{(i)} \delta(t-t') \quad (2.28)$$

The Brownian force term can be decomposed as (10)

$$\left[ \underline{\underline{\zeta}}^{(i)} \right]^{-1} \cdot \underline{F}_B^{(i)} = \frac{F_{B,\square}^{(i)}}{\zeta_{\square}^{(i)}} \underline{p}^{(i)} + \frac{F_{B,\perp 1}^{(i)}}{\zeta_{\perp 1}^{(i)}} \underline{p}_{\perp 1}^{(i)} + \frac{F_{B,\perp 2}^{(i)}}{\zeta_{\perp 2}^{(i)}} \underline{p}_{\perp 2}^{(i)} \quad (2.29)$$

where the forces  $F_{B,\square}^{(i)}$ ,  $F_{B,\perp 1}^{(i)}$  and  $F_{B,\perp 2}^{(i)}$  are the Brownian forces and drag coefficients parallel and perpendicular to the orientation of the ellipsoids with magnitude

$$F_{B,\square}^{(i)} = \zeta_{\square}^{(i)} \sqrt{\frac{2 \cdot d \cdot D_{T,\square}^{(i)}}{\Delta t}} \quad (2.30)$$

$$F_{B,\perp 1}^{(i)} = \zeta_{\perp 1}^{(i)} \sqrt{\frac{2 \cdot d \cdot D_{T,\perp 1}^{(i)}}{\Delta t}} \quad (2.31)$$

$$F_{B,\perp 2}^{(i)} = \zeta_{\perp 2}^{(i)} \sqrt{\frac{2 \cdot d \cdot D_{T,\perp 2}^{(i)}}{\Delta t}} \quad (2.32)$$

and the translational drag and diffusion coefficients are given by

$$\zeta_{\square}^{(i)} = \eta X_A^{(i)} \quad (2.33)$$

$$\zeta_{\perp 1}^{(i)} = \zeta_{\perp 2}^{(i)} = \zeta_{\perp}^{(i)} = \eta Y_A^{(i)} \quad (2.34)$$

$$D_{T,\square}^{(i)} = \frac{kT}{\zeta_{\square}^{(i)}} \quad (2.35)$$

$$D_{T,\perp 1}^{(i)} = D_{T,\perp 2}^{(i)} = \frac{kT}{\zeta_{\perp}^{(i)}} \quad (2.36)$$

The orientation vectors  $\underline{p}_{\perp 1}^{(i)}$  and  $\underline{p}_{\perp 2}^{(i)}$  are given in Appendix A.

In a similar manner, the Brownian term for the torque can be decomposed as

$$\left[ \underline{\underline{\xi}}^{(i)} \right]^{-1} \cdot \underline{T}_B^{(i)}(t) = \frac{\mathbf{T}_{B,\square}^{(i)}}{\xi_{\square}^{(i)}} \underline{p}^{(i)} + \frac{\mathbf{T}_{B,\perp 1}^{(i)}}{\xi_{\perp 1}^{(i)}} \underline{p}_{\perp 1}^{(i)} + \frac{\mathbf{T}_{B,\perp 2}^{(i)}}{\xi_{\perp 2}^{(i)}} \underline{p}_{\perp 2}^{(i)} \quad (2.37)$$

where the torques  $\mathbf{T}_{B,\square}^{(i)}$ ,  $\mathbf{T}_{B,\perp 1}^{(i)}$  and  $\mathbf{T}_{B,\perp 2}^{(i)}$  are the Brownian torques parallel and perpendicular to the orientation of the ellipsoids with magnitude

$$\mathbf{T}_{B,\square}^{(i)} = \xi_{\square}^{(i)} \sqrt{\frac{2 \cdot d \cdot D_{R,\square}^{(i)}}{\Delta t}} \quad (2.38)$$

$$\mathbf{T}_{B,\perp 1}^{(i)} = \xi_{\perp 1}^{(i)} \sqrt{\frac{2 \cdot d \cdot D_{R,\perp 1}^{(i)}}{\Delta t}} \quad (2.39)$$

$$\mathbf{T}_{B,\perp 2}^{(i)} = \xi_{\perp 2}^{(i)} \sqrt{\frac{2 \cdot d \cdot D_{R,\perp 2}^{(i)}}{\Delta t}} \quad (2.40)$$

and the rotational drag and diffusion coefficients are given by

$$\xi_{\square}^{(i)} = \eta X_C^{(i)} \quad (2.41)$$

$$\xi_{\perp 1}^{(i)} = \xi_{\perp 2}^{(i)} = \xi_{\perp}^{(i)} = \eta Y_C^{(i)} \quad (2.42)$$

$$D_{R,\square}^{(i)} = \frac{kT}{\xi_{\square}^{(i)}} \quad (2.43)$$

$$D_{R,\perp 1}^{(i)} = D_{R,\perp 2}^{(i)} = \frac{kT}{\xi_{\perp}^{(i)}} \quad (2.44)$$

### Model for flow-FFF

In flow-FFF, the fluid velocity vector has two non-zero components,  $\underline{v} = [v_x, v_y, 0]$ . The x-velocity is given by

$$v_x = \frac{h^2}{2\eta} \left( -\frac{\partial P}{\partial x} \right) \left[ 1 - \frac{y^2}{h^2} \right] \quad (2.45)$$

where  $h$  is the half gap width, and  $v_y = f(t)$ , where  $f(t)$  is a function that is uniform in the spatial dimensions, but which can be a function of time. Under these conditions, and after some simplifying assumptions, the governing equations for the fiber motion are given by

$$\frac{dR_x^{(i)}}{dt} = v_x + \left( \frac{F_{B,\square}^{(i)}}{\xi_{\square}^{(i)}} p_x^{(i)} + \frac{F_{B,\perp 1}^{(i)}}{\xi_{\perp 1}^{(i)}} p_{\perp 1,x}^{(i)} + \frac{F_{B,\perp 2}^{(i)}}{\xi_{\perp 2}^{(i)}} p_{\perp 2,x}^{(i)} \right) \quad (2.46)$$

$$\frac{dR_y^{(i)}}{dt} = v_y + \left( \frac{F_{B,\square}^{(i)}}{\xi_{\square}^{(i)}} p_y^{(i)} + \frac{F_{B,\perp 1}^{(i)}}{\xi_{\perp 1}^{(i)}} p_{\perp 1,y}^{(i)} + \frac{F_{B,\perp 2}^{(i)}}{\xi_{\perp 2}^{(i)}} p_{\perp 2,y}^{(i)} \right) \quad (2.47)$$

$$\frac{dR_z^{(i)}}{dt} = v_z + \left( \frac{F_{B,\square}^{(i)}}{\xi_{\square}^{(i)}} p_z^{(i)} + \frac{F_{B,\perp 1}^{(i)}}{\xi_{\perp 1}^{(i)}} p_{\perp 1,z}^{(i)} + \frac{F_{B,\perp 2}^{(i)}}{\xi_{\perp 2}^{(i)}} p_{\perp 2,z}^{(i)} \right) \quad (2.48)$$

$$\frac{d}{dt}(p_x^{(i)}) = \frac{1}{2} \frac{\partial v_x}{\partial y} p_y^{(i)} \left[ 1 + \lambda (1 - 2p_x^{(i)} p_x^{(i)}) \right] + \left( \frac{\mathbf{T}_{B,\perp 2}^{(i)}}{\xi_{\perp 2}^{(i)}} p_{\perp 1,x}^{(i)} - \frac{\mathbf{T}_{B,\perp 1}^{(i)}}{\xi_{\perp 1}^{(i)}} p_{\perp 2,x}^{(i)} \right) \quad (2.49)$$

$$\frac{d}{dt}(p_y^{(i)}) = \frac{1}{2} \frac{\partial v_x}{\partial y} p_x^{(i)} \left[ -1 + \lambda (1 - 2p_y^{(i)} p_y^{(i)}) \right] + \left( \frac{\mathbf{T}_{B,\perp 2}^{(i)}}{\xi_{\perp 2}^{(i)}} p_{\perp 1,y}^{(i)} - \frac{\mathbf{T}_{B,\perp 1}^{(i)}}{\xi_{\perp 1}^{(i)}} p_{\perp 2,y}^{(i)} \right) \quad (2.50)$$

$$\frac{d}{dt}(p_z^{(i)}) = -\lambda p_x^{(i)} p_y^{(i)} p_z^{(i)} \frac{\partial v_x}{\partial y} + \left( \frac{\mathbf{T}_{B,\perp 2}^{(i)}}{\xi_{\perp 2}^{(i)}} p_{\perp 1,z}^{(i)} - \frac{\mathbf{T}_{B,\perp 1}^{(i)}}{\xi_{\perp 1}^{(i)}} p_{\perp 2,z}^{(i)} \right) \quad (2.51)$$

where the velocity gradient is given by

$$\frac{\partial v_x}{\partial y} = -\frac{y}{\eta} \left( -\frac{\partial P}{\partial x} \right) \quad (2.52)$$

Equations (2.46)-(2.51) constitute the model equations used to solve for the particle dynamics

in flow-FFF. These are integrated forward in time for each particle in the ensemble based on initial conditions for particle position and orientation.

## Results

### Diffusion Calculations

In order to test the algorithm, Brownian Dynamics simulations were carried out for ellipsoidal particles in the absence of flow for two cases. In the first case, the particles were allowed to freely translate and rotate. Although the particles are anisotropic, in the absence of flow they experience all orientations equally, and thus, the effective diffusion coefficient is isotropic. An approximate analytical solution for the effective diffusion coefficient in this case has been derived by Perrin (15), and is given by

$$D = \frac{\left(\frac{kT}{6\pi\eta a}\right)}{\sqrt{1-\left(\frac{b}{a}\right)^2}} \ln \left[ \frac{1 + \sqrt{1-\left(\frac{b}{a}\right)^2}}{\left(\frac{b}{a}\right)} \right] \quad (3.1)$$

Comparison of simulation values with the approximate analytical solution (15) for the effective diffusion coefficient are shown in Table 2, and the values for the two cases fall within 3-10% of each other.

$a$ (m)	$b$ (m)	$\Re$	$D_{eff}(m^2/s),$ <i>Perrin</i>	$D_{eff}(m^2/s),$ <i>Simulation</i>	% Difference
$2 \times 10^{-7}$	$1 \times 10^{-7}$	2	$1.63 \times 10^{-12}$	$1.69 \times 10^{-12}$	3.77
$2 \times 10^{-6}$	$1 \times 10^{-7}$	20	$3.96 \times 10^{-13}$	$4.28 \times 10^{-13}$	7.95
$2 \times 10^{-5}$	$1 \times 10^{-7}$	200	$6.43 \times 10^{-14}$	$7.06 \times 10^{-14}$	9.85

Table 2 – Comparison of effective diffusion coefficients computed by the simulation with the approximate analytical solution of Perrin (15) for an ensemble of  $N = 1000$  particles.

Diffusion at fixed particle orientations was also examined, and it was determined that the particles diffuse in the correct anisotropic manner with the correct magnitude along the coordinate axes. Simulation results for particles diffusing at a fixed angle of  $45^\circ$  with the model values are compared in Table 3.

$a$ (m)	$b$ (m)	$D_{xx}(m^2/s),$ <i>Model</i>	$D_{yy}(m^2/s),$ <i>Model</i>	$D_{xx}(m^2/s),$ <i>Simulation</i>	$D_{yy}(m^2/s),$ <i>Simulation</i>	Max Difference
$2 \times 10^{-5}$	$1 \times 10^{-7}$	$7.03 \times 10^{-14}$	$7.03 \times 10^{-14}$	$7.02 \times 10^{-14}$	$6.99 \times 10^{-14}$	5%

Table 3 – Comparison between the model and simulation values for the diffusion coefficients along the coordinate axes for the diffusion of prolate ellipsoids at a fixed orientation of  $45^\circ$  for an ensemble of  $N = 1000$  particles.

Together, the two diffusion cases examined show that the Brownian motion of the particles is being computed in the correct manner.

### ***Solution of Jeffery's Equation***

The solution algorithm for Jeffery's equation was also tested. For a particle in 2-D, steady shear flow in the absence of Brownian motion, there is an analytical solution describing for the orientation and period for the in-plane rotation of the particles (16). The solution for the period is given as

$$T = \frac{2\pi}{\dot{\gamma}} \left( \mathfrak{R} + \frac{1}{\mathfrak{R}} \right) \quad (3.2)$$

Simulation results were compared with the analytical solution for a variety of parameter conditions and the results were found to be virtually indistinguishable at all particle aspect ratios above 10. Results for the orientation with  $\mathfrak{R} = 20$  and  $\dot{\gamma} = 10 s^{-1}$ , and no rotational diffusion are shown in Figure 7. The value of the period calculated from the simulation of  $T = 12.6 s$  compares very well with the analytical value of  $T = 4.01\pi s = 12.598 s$ .

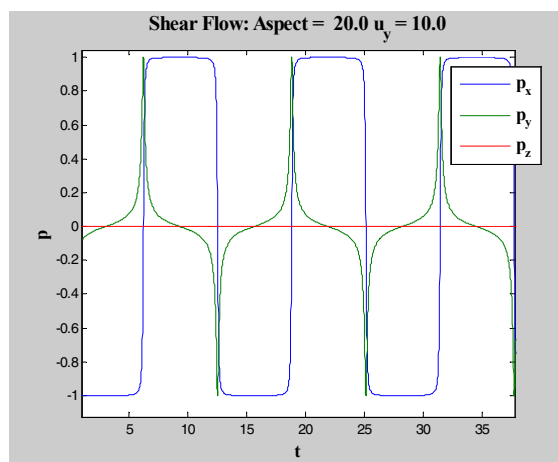


Figure 7 – Simulation of Jeffery's equation for the orientation at  $\mathfrak{R} = 20$  and  $\dot{\gamma} = 10 s^{-1}$ .

The results for the solution of Jeffery's equation in non-Brownian systems shows that at high aspect ratios the particles are mostly aligned in the flow direction and quickly flip every half period. A solution to Jeffery's equation for stochastic systems is shown in Figure 8. The average period and in-plane orientation is similar to that for non-Brownian systems, with the main difference being that particles tend to “kayak” out of plane when they flip. In terms of application to FFF, this shows that the diffusion which governs the particle retention should be described in terms of the transverse diffusion coefficient of the model, as the particles spend the majority of the time oriented in the flow direction.

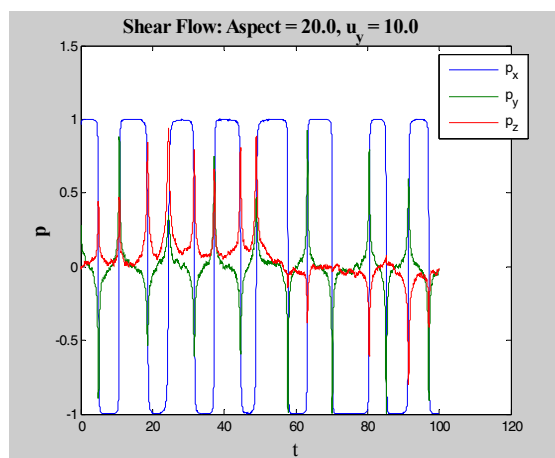


Figure 8 – Simulation of Jeffery’s equation with Brownian motion for the orientation at  $\mathfrak{R} = 20$  and  $\dot{\gamma} = 10 s^{-1}$ .

### Modeling of Flow-FFF

An example a simulation of ellipsoids in flow-FFF is shown in Figure 9, for the parameters shown in Table 4. The solution is assumed to be aqueous at 293 K. The particles are all started from the same initial point at the channel entrance just above the lower wall to mimic the experimental practice of focusing<sup>d</sup>. The dispersion of the particles due to the random Brownian motion is evident.



Figure 9 – Startup flow showing dispersion (spreading) of ellipsoids in flow-FFF for a uniform mixture with  $\mathfrak{R} = 100$  and  $N = 1000$  particles. All particles start from identical initial positions. Dispersion occurs due to the interplay between the transverse diffusion and the parabolic velocity field.

$a$ (m)	$b$ (m)	$L$ (m)	$W$ (m)	$H$ (m)	$Q_x$ ( $m^3/s$ )	$Q_y$ ( $m^3/s$ )
$1 \times 10^{-7}$	$1 \times 10^{-9}$	0.2	0.1	0.001	$2 \times 10^{-9}$	$2 \times 10^{-9}$

Table 4 – Parameters used for simulation in Figures 9-10.

The elution profile for the simulation is shown in Figure 10. The distribution has a slight negative skewness about the mean. The statistics of the distribution are shown in Table 5 and compared with the values for the theoretical minimum residence and retention times. The transverse diffusion coefficient of the ellipsoids was used to calculate the Retention. The minimum simulated transit time is quite close to the theoretical minimum, but the maximum is much larger than the

<sup>d</sup> In practice, the sample to be separated in FFF is injected into the channel and the flow is initially run in reverse so that the initially circular injection spot is compressed into a band at the entrance gate. Focusing narrows the elution peaks.

theoretical retention time. Thus, the simulated distribution is quite a bit broader than that based on theory.

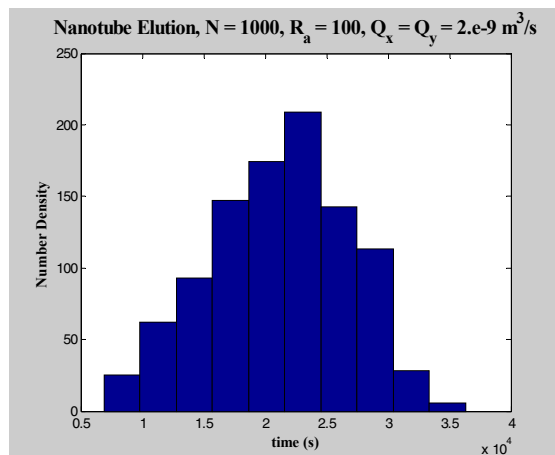


Figure 10 – Elution histogram for the flow-FFF simulation of a uniform mixture of ellipsoids with  $\mathfrak{R} = 100$  and  $N = 1000$  particles.

<i>Theory</i>				<i>Simulation</i>			
Retention	$t_{min}$ (s)	$t_0$ (s)	$t_r$ (s)	Mean (s)	Standard Deviation (s)	Min (s)	Max (s)
0.527	6667	13333	25285	21163	5638	6870	36302

Table 5 – Comparison of theoretical and simulated residence times for the simulation in Figures 9-10.

### Summary and Conclusion

A Brownian dynamics simulation for the flow of dilute ellipsoids has been developed to model the separation of nanotubes in flow-FFF. The particle motions are governed by stochastic forms of a linear momentum balance with orientation dependent drag and diffusion coefficients, and the Jeffery equation with rotational diffusion. The simulation was tested by comparing results for Brownian diffusion of prolate ellipsoids with theoretical results, and with analytical results for Jeffery’s equation in shear flow. The simulation of Jeffery’s equation showed that high aspect ratio particles stay oriented in shear for long periods of time even with Brownian diffusion, and thus, the Retention for spheres should be described in terms of the transverse diffusion coefficient of the particle. The simulation of flow-FFF for nanotube scale particles shows that they elute by a normal mode mechanism, based on a particle diameter of 1 nm. Further exploration of the parameter space (ongoing) is needed in order to draw broader conclusions.

The results shown here do allow one to draw the conclusion that conventional flow-FFF can be expected to drive length based separation of nanotubes. However, it is also desirable to separate them according to their electronic properties or chirality. In normal mode operation, the ability to separate particles depends on the relative Retention values of the different particles. In future work, we will use the simulation to investigate whether a modification of conventional flow-FFF with either electric or

magnetic fields can be used as a basis for separating tubes according to their electronic properties. For example, selective orientation of metallic tubes, or differences in electrophoretic mobility between metallic and semi-conducting tubes could be a basis for creating retention differences between these different species, and thus promoting separation.

## References

### References

1. Giddings, J. C., "Field-Flow Fractionation - Analysis of Macromolecular, Colloidal, and Particulate Materials," *Science*, Vol. 260, No. 5113, 1993, pp. 1456-1465.
2. *Field-Flow Fractionation Handbook*, Wiley-Interscience 2000.
3. Janca, J., *Field-Flow Fractionation*, Marcel Dekker, New York, 1987.
4. Chen, B. L. and Selegue, J. P., "Separation and characterization of single-walled and multiwalled carbon nanotubes by using flow field-flow fractionation," *Analytical Chemistry*, Vol. 74, No. 18, 2002, pp. 4774-4780.
5. Moon, M. H., Kang, D. J., Jung, J. H., and Kim, J. M., "Separation of carbon nanotubes by frit inlet asymmetrical flow field-flow fractionation," *Journal of Separation Science*, Vol. 27, No. 9, 2004, pp. 710-717.
6. Selegue, J. P., Chen, B. L., Wijeratne, L., Meier, M. S., Wang, Z. W., Haddon, R. C., Hu, H., and Andrews, R., "Field-flow fractionation of single- and multi-walled carbon nanotubes," *Abstracts of Papers of the American Chemical Society*, Vol. 222, 2001, pp. U524.
7. Tagmatarchis, N., Zattoni, A., Reschiglian, P., and Prato, M., "Separation and purification of functionalised water-soluble multi-walled carbon nanotubes by flow field-flow fractionation," *Carbon*, Vol. 43, No. 9, 2005, pp. 1984-1989.
8. Peng, H. Q., Alvarez, N. T., Kittrell, C., Hauge, R. H., and Schmidt, H. K., "Dielectrophoresis field flow fractionation of single-walled carbon nanotubes," *Journal of the American Chemical Society*, Vol. 128, No. 26, 2006, pp. 8396-8397.
9. Liu, J., Rinzler, A. G., Dai, H. J., Hafner, J. H., Bradley, R. K., Boul, P. J., Lu, A., Iverson, T., Shlimov, K., Huffman, C. B., Rodriguez-Macias, F., Shon, Y. S., Lee, T. R., Colbert, D. T., and Smalley, R. E., "Fullerene pipes," *Science*, Vol. 280, No. 5367, 1998, pp. 1253-1256.
10. Satoh, A., *Introduction to Molecular-Microsimulation of Colloidal Dispersions*, Elsevier Science B.V., Amsterdam, The Netherlands, 2003.
11. Kim, S. and Karrila, S. J., *Microhydrodynamics: Principles and selected applications*, Butterworth-Heinemann, Stoneham, 1991.
12. Ausias, G., Fan, X. J., and Tanner, R. I., "Direct simulation for concentrated fibre suspensions in

transient and steady state shear flows," *Journal of Non-Newtonian Fluid Mechanics*, Vol. 135, 2006, pp. 46-57.

13. Cobb, P. D. and Byron, C., "Simulations of concentrated suspensions of rigid fibers: relationship between short-time diffusivities and the long-time rotational diffusion," *Journal of Chemical Physics*, Vol. 123, 2005, pp. 054908-1-054908-19.
14. Dhont, J. K. G. and Briels, W. J., "Viscoelasticity of suspensions of long, rigid rods," *Colloids and Surfaces A-Physicochemical and Engineering Aspects*, Vol. 213, 2003, pp. 131-156.
15. Perrin, F., "Mouvement brownien d'un ellipsoïde: (II) Rotation libre et depolarisation des fluorescences. Translation et diffusion de molécules ellipsoïdales," *Journal de Physique et le Radium*, Vol. 7, 1936, pp. 1-11.
16. Jeffery, G. B., "The motion of ellipsoidal particles immersed in a viscous fluid," *Proceedings of the Royal Society of London*, Vol. Series A 102, 1922, pp. 161-179.

## Appendix A – Orientation Vectors

If the orientation vector  $\underline{p} = [p_x, p_y, p_z]$  is renormalized such that

$$\underline{p} = \frac{1}{\alpha} [p_x, p_y, p_z] \quad (4.1)$$

where  $\alpha = \sqrt{p_x^2 + p_y^2 + p_z^2}$ , then the components of the orientation vectors  $\underline{p}_{\perp 1}$  and  $\underline{p}_{\perp 2}$  are given by

$$\underline{p}_{\perp 1} = \left[ \frac{-p_y}{\sqrt{p_x^2 + p_y^2}}, \frac{p_x}{\sqrt{p_x^2 + p_y^2}}, 0 \right] \quad (4.2)$$

$$\underline{p}_{\perp 2} = \left[ \frac{-p_x p_z}{\alpha \sqrt{p_x^2 + p_y^2}}, \frac{-p_y p_z}{\alpha \sqrt{p_x^2 + p_y^2}}, \frac{p_x^2 + p_y^2}{\alpha \sqrt{p_x^2 + p_y^2}} \right] \quad (4.3)$$